Draft version April 18, 2019
Typeset using LaTeX **preprint** style in AASTeX61

DISCOVERY OF AN INTERMEDIATE-LUMINOSITY RED TRANSIENT IN M51 AND ITS LIKELY DUST-OBSCURED, INFRARED-VARIABLE PROGENITOR

Jacob E. Jencson,[1] Scott M. Adams,[1] Howard E. Bond,[2,3] Schuyler D. van Dyk,[4]
Mansi M. Kasliwal,[1] John Bally,[5] Nadejda Blagorodnova,[6] Kishalay De,[1]
Christoffer Fremling,[1] Yuhan Yao,[1] Andrew Fruchter,[3] David Rubin,[3] Cristina Barbarino,[7]
Jesper Sollerman,[7] Adam A. Miller,[8] Erin K. S. Hicks,[9] Matthew A. Malkan,[10] Igor Andreoni,[1]
Eric C. Bellm,[11] Richard Dekany,[12] Michael Feeney,[12] Sara Frederick,[13] Avishay Gal-Yam,[14]
Robert D. Gehrz,[15] Matteo Giomi,[16] Matthew J. Graham,[1] David Hale,[12] Matthew J. Hankins,[1]
George Helou,[4] Anna Y. Q. Ho,[1] T. Hung,[17] Mario Jurić,[11] S. R. Kulkarni,[1] Ryan M. Lau,[18]
Frank J. Masci,[4] James D. Neill,[1] Reed L. Riddle,[12] Ben Rusholme,[4] Nathan Smith,[19]
Roger M. Smith,[12] Maayane T. Soumagnac,[20] Yutaro Tachibana,[21,1] Samaporn Tinyanont,[1]
Richard Walters,[12] and Robert E. Williams[3,17]

[1]*Division of Physics, Mathematics, and Astronomy, California Institute of Technology, Pasadena, CA 91125, USA*
[2]*Department of Astronomy & Astrophysics, Pennsylvania State University, University Park, PA 16802, USA*
[3]*Space Telescope Science Institute, 3700 San Martin Dr., Baltimore, MD 21218, USA*
[4]*Caltech/IPAC, Mailcode 100-22, Pasadena, CA 91125, USA*
[5]*Center for Astrophysics and Space Astronomy, University of Colorado, 389 UCB, Boulder, CO 80309, USA*
[6]*Department of Astrophysics/IMAPP, Radboud University, Nijmegen, The Netherlands*
[7]*The Oskar Klein Centre, Department of Astronomy, Stockholm University, AlbaNova, SE-106 91 Stockholm, Sweden*
[8]*Center for Interdisciplinary Exploration and Research in Astrophysics (CIERA) and Department of Physics and Astronomy, Northwestern University, Evanston, IL 60208, USA*
[9]*University of Alaska Anchorage, 3211 Providence Drive, Anchorage, AK 99508*
[10]*University of California Los Angeles, Department of Astronomy & Astrophysics, 430 Portola Plaza, Box 951547, Los Angeles, CA 90095-1547*
[11]*DIRAC Institute, Department of Astronomy, University of Washington, 3910 15th Avenue NE, Seattle, WA 98195, USA*
[12]*Caltech Optical Observatories, California Institute of Technology, Pasadena, CA 91125*
[13]*Department of Astronomy, University of Maryland, College Park, MD 20742, USA*
[14]*Department of Particle Physics and Astrophysics, Weizmann Institute of Science, Rehovot 76100, Israel*
[15]*Minnesota Institute for Astrophysics, School of Physics and Astronomy, University of Minnesota, 116 Church Street, S. E., Minneapolis, MN 55455, USA*
[16]*Humboldt-Universität zu Berlin, Newtonstraße 15, 12489 Berlin, Germany*
[17]*Department of Astronomy and Astrophysics, University of California, Santa Cruz, CA 95064, USA*
[18]*Institute of Space & Astronautical Science, Japan Aerospace Exploration Agency, 3-1-1 Yoshinodai, Chuo-ku, Sagamihara,Kanagawa 252-5210, Japan*
[19]*University of Arizona, Steward Observatory, 933 N. Cherry Avenue, Tucson, AZ 85721, USA*
[20]*Benoziyo Center for Astrophysics, Weizmann Institute of Science, Rehovot, Israel*
[21]*Department of Physics, Tokyo Institute of Technology, 2-12-1 Ookayama, Meguro-ku, Tokyo 152-8551, Japan*

ABSTRACT

Corresponding author: Jacob E. Jencson
jj@astro.caltech.edu

We present the discovery of an optical transient (OT) in Messier 51, designated M51 OT2019-1 (also ZTF 19aadyppr, AT 2019abn, ATLAS19bzl), by the Zwicky Transient Facility (ZTF). The OT rose over 15 days to an observed plateau luminosity of $M_r = -13$ ($\nu L_\nu = 9 \times 10^6\ L_\odot$), in the luminosity gap between novae and supernovae (SNe). The spectral sequence shows a red continuum, prominent Balmer emission with a velocity width of $\approx 400\,\mathrm{km\,s^{-1}}$, Ca II and [Ca II] emission, and absorption features (Ca II H+K, Na I D, O I 7773 Å blend) characteristic of an F-type supergiant spectrum. The properties of spectra and multi-band light curves are similar in many ways to the so-called "SN impostors" and intermediate-luminosity red transients (ILRTs). We directly identify the likely progenitor in archival *Spitzer Space Telescope* imaging with a 4.5 μm luminosity of $M_{[4.5]} \approx -12.2$ mag and a $[3.6]-[4.5]$ color redder than 0.74 mag, similar to those of the prototype ILRTs SN 2008S and NGC 300 OT2008-1. Intensive monitoring of M51 with *Spitzer* further reveals evidence for significant variability of the progenitor candidate at [4.5] in the years before the OT. There is no identifiable counterpart at the location of the OT in archival *Hubble Space Telescope* imaging. The optical colors combined with spectroscopic temperature constraints imply a higher reddening of $E(B-V) \approx 0.7$ mag and higher intrinsic luminosity of $M_r \approx -14.9$ mag ($\nu L_\nu = 5.3 \times 10^7\ L_\odot$) on the plateau than seen in previous ILRT candidates. Moreover, the extinction estimate is higher on the rise than on the plateau, suggestive of an extended phase of circumstellar dust destruction. These results, enabled by the early discovery of M51 OT2019-1 and extensive pre-outburst archival coverage, offer new clues about the debated origins of ILRTs and may challenge the hypothesis that they arise from the electron-capture induced collapse of extreme asymptotic-giant-branch stars.

Keywords: galaxies: individual (M51), stars: supernovae: individual (M51 OT2019-1), stars: variables: general, stars: evolution, stars: circumstellar matter, stars: winds, outflows

1. INTRODUCTION

Searches for transients in the nearby universe have uncovered a diverse array of hydrogen-rich stellar events occupying the luminosity range between that of novae and supernovae (SNe). As more well-characterized events have been found, some defined classes are beginning to emerge. Distinguishing among these classes, however, can be challenging as there is significant overlap in their observed properties. These include events often associated with luminous blue variables (LBVs; Humphreys & Davidson 1994; Smith & Owocki 2006) variably referred to as "SN impostors," "η Carinae variables," or "giant eruptions" (Humphreys et al. 1999; Van Dyk et al. 2000; Smith et al. 2010; Pastorello et al. 2010; Smith 2014). The "luminous red novae" (LRNe) are believed to be associated with stellar mergers or common-envelope ejections, including the 1–3 $M_\odot$ contact-binary merger V1309 Sco (Tylenda et al. 2011) and the B-type stellar merger V838 Mon (Bond et al. 2003; Sparks et al. 2008). Several extragalactic events are also suggested to be members of this class, e.g., M31 RV (Rich et al. 1989; Bond & Siegel 2006; Bond 2011), M85 OT2006-1 (Kulkarni et al. 2007), NGC 4490 OT2011-1 (Smith et al. 2016), and M101 OT2015-1 (Blagorodnova et al. 2017).

We adopt the term "intermediate-luminosity red transient" (ILRT), originally suggested by Bond et al. (2009), to refer to the class of SN impostors similar to two well-characterized prototypes: SN 2008S (Prieto et al. 2008; Botticella et al. 2009; Smith et al. 2009) and the 2008 optical transient (OT) in NGC 300 (NGC 300 OT2008-1; Bond et al. 2009; Berger et al. 2009; Humphreys et al. 2011). As the name suggests, these events reach peak luminosities ($M_{r/R} \approx -13$ to -14) fainter than those of typical core-collapse SNe, but comparable to those of other impostors. The peak is followed by the monotonic decline of their optical light curves, and they also show reddened spectra suggestive of strong internal extinction from the immediate circumburst environment. Their spectra are similar to some LBV-related transients and LRNe, showing strong H, Ca II, and rare [Ca II] emission features superimposed on an absorption spectrum characteristic of an F-type supergiant. The intermediate-width H features indicate relatively low ejection velocities of a few $\times$ 100 km s^{-1}. Both NGC 300 OT2008-1 and SN 2008S had densely self-obscured progenitor stars detected in archival imaging with the *Spitzer Space Telescope*, whose luminosities and inferred masses ($M \approx$ 9–15 $M_\odot$; Prieto 2008; Prieto et al. 2008; Thompson et al. 2009; Kochanek 2011) are lower than those of classical LBVs. Both events have now faded below their pre-explosion luminosities in the IR (Adams et al. 2016), suggesting that the explosions may have been terminal. Other proposed members of this class discovered in the last decade include PTF 10fqs (Kasliwal et al. 2011), SN 2010dn (Smith et al. 2011), and AT 2017be (Cai et al. 2018), although their larger distances prevented the direct identification of progenitors.

We present the discovery by the Zwicky Transient Facility (ZTF) of an OT in M51 with similar properties to those of previously observed ILRTs and other SN impostors. At a distance of only 8.6 Mpc (McQuinn et al. 2016, 2017), this is the closest such event in over a decade, allowing us to identify and characterize a candidate progenitor star in archival *Spitzer* images. In this letter, we describe the discovery and early observations (Section 2), our analysis of the available archival imaging and identification of the likely progenitor (Section 3.1), the early photometric (Section 3.2) and spectroscopic (Section 3.3) evolution. In Section 4, we discuss the properties of the OT and its progenitor in the context of similar transients, and suggest it is a member of the ILRT class offering new insights on their origins.

2. DISCOVERY AND DATA COLLECTION

2.1. *Discovery in M51*

On UT 2019 January 22.6 (MJD = 58505.6), ZTF 19aadyppr was detected as a new OT source in the nearby galaxy M51 by the Zwicky Transient Facility (ZTF; Bellm et al. 2019; Graham et al. 2019) with the 48-inch Samual Oschin Telescope (P48) at Palomar Observatory as part of the public ZTF 3-day cadence survey of the visible Northern Sky. The detection passed significance (Masci et al. 2019) and machine-learning thresholds (Mahabal et al. 2019; Tachibana & Miller 2018), and was released as a public alert (Patterson et al. 2019). We refer to the phase, t, as the number of days since the first ZTF detection throughout this work. Located at a right ascension and declination of $13^{\mathrm{h}}29^{\mathrm{m}}42\overset{\mathrm{s}}{.}41, +47^{\circ}11'16\overset{''}{.}6$ (J2000.0), the source had an r-band AB magnitude at first detection of 19.6 ± 0.2. The source was not detected in an earlier image taken on 2019 January 19.6, to a limiting magnitude of $r > 20.5$, at $t = -3$ days. After a second detection on 2019 January 25.5 (MJD = 58508.5), ZTF 19aadyppr was autonomously selected as a high-quality transient by the AMPEL analysis framework (Nordin et al. 2019b). The discovery was submitted to the Transient Name Server and provided the IAU designation AT 2019abn (Nordin et al. 2019a). The source passed several ZTF science-program filters and was saved by human scanners for follow-up on the GROWTH Marshal (Kasliwal et al. 2019). Early spectroscopic observations reported by De et al. (2019) on 2019 January 26 were characterized by a red continuum and strong, intermediate-width (≈ 600 km s^{-1}) Hα emission, consistent with a classification of SN impostor or young ILRT. An independent detection was reported to TNS on 2019 January 26 by the the ATLAS survey (Tonry et al. 2018), and the Las Cumbres Observatory (LCO) Global SN Project reported an additional spectrum taken on 2019 March 2 (Burke et al. 2019) and ILRT classification. We use the name M51 OT2019-1 for this event hereafter.

As shown in Figure 1, the transient was located in a star-forming spiral arm of M51, $108\overset{''}{.}2$ from the galaxy's center. There is a prominent dust lane at the site, indicating the source may be subject to significant host extinction. Notably, M51 has a high rate of core-collpase SNe, with 3 known events discovered in the last 25 years: SN 1994I (type Ic; Schmidt et al. 1994), SN 2005cs (type II; Modjaz et al. 2005), and SN 2011dh (type IIb; Silverman et al. 2011). The NASA/IPAC Extragalactic Database[1] (NED) lists 50 individual distance measurements to M51, with a median value in distance modulus of 29.5 mag and a large standard deviation of 0.9 mag. Throughout this work we assume a distance modulus for M51 from McQuinn et al. (2016, 2017) of $m - M = 29.67 \pm 0.02$ (statistical) ± 0.07 (systematic; Rizzi et al. 2007) mag based on the luminosity of the tip of the red-giant branch (TRGB) method, and that the systematic uncertainties associated with calibrating this method dominate over the statistical measurement uncertainties. We adopt the value from NED for the Galactic extinction towards M51 of $E(B-V) = 0.03$ mag, based on the Schlafly & Finkbeiner (2011) recalibration of Schlegel et al. (1998), and assuming a standard (Fitzpatrick 1999) reddening law with $R_V = 3.1$.

2.2. *Imaging observations*

The field containing M51 OT2019-1 was regularly observed at several epochs with the ZTF camera on P48 in the g, r, and i bands. The P48 images were reduced with the ZTF Science Data System pipelines (Masci et al. 2019), which performs point-spread-function (PSF) photometry on the reference-subtracted images. We utilize this photometry for data from the public ZTF survey. For images taken as part of the ZTF Collaboration surveys and the Caltech surveys (Bellm et al 2019b, PASP in press), we subsequently performed forced PSF-fitting photometry at the location of M51 OT2019-1, adopting a linear model for pixel values in the difference images as a function of the normalized PSF-model image values and use

---

[1] NED is operated by the Jet Propulsion Laboratory, California Institute of Technology, under contract with the National Aeronautics and Space Administration.

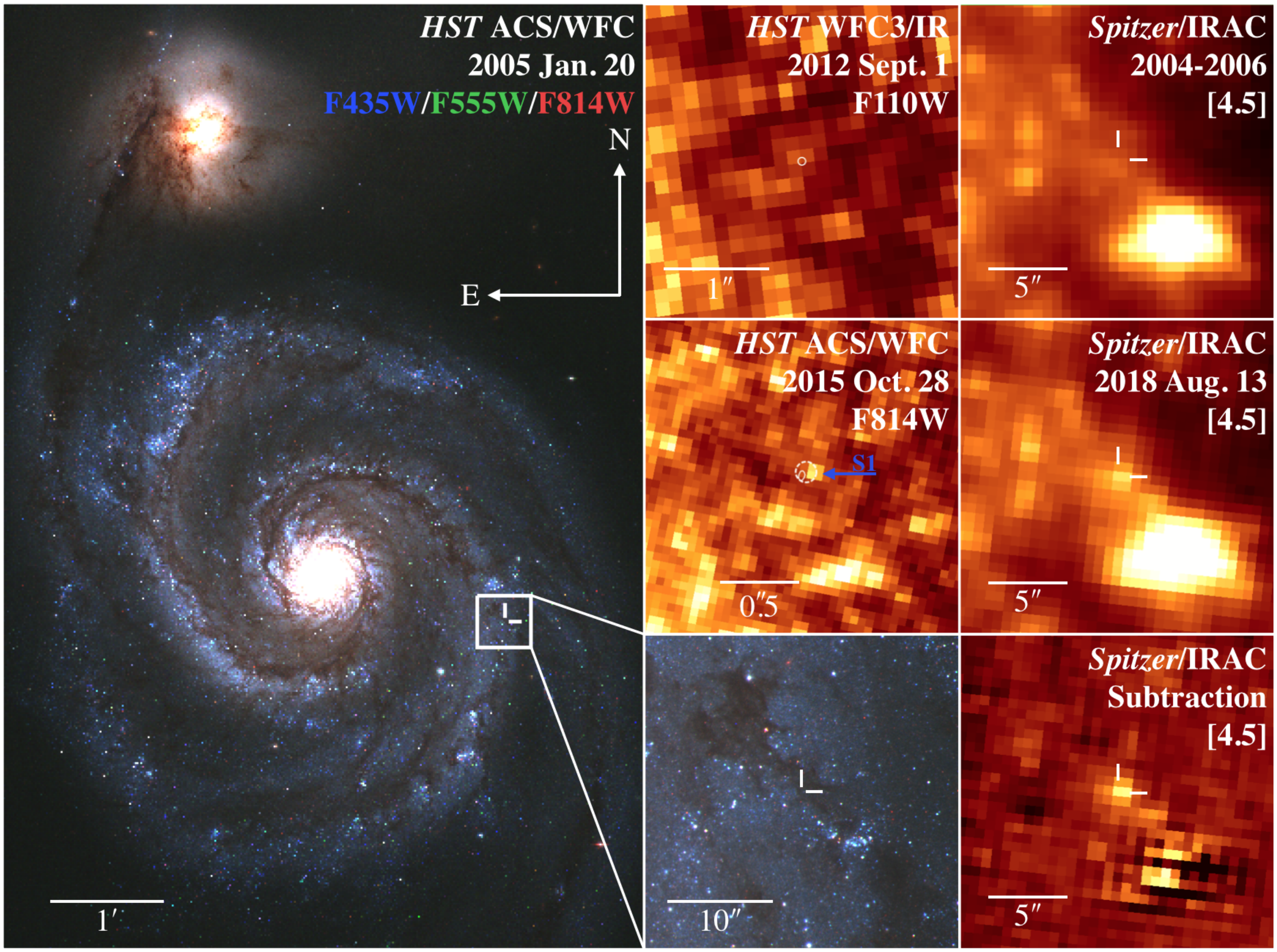

Figure 1. Pre-explosion *HST* and *Spitzer* imaging of M51 OT2019-1. In the leftmost panel, we show the color-composite *HST* ACS/WFC mosaics of the M51 system from 2005 in three filters (F435W in blue, F555W in green, and F814W in red; PID: GO-10451; PI: S. Beckwith). The location of M51 OT2019-1 in a prominent dust lane along a spiral arm is indicated by the white cross-hairs and shown in more detail in the $30'' \times 30''$ bottom-center zoom-in panel. Above in the center column, we show the archival *HST* coverage of the site in 2015 with ACS/WFC in F814W (center row) and in 2012 with WFC3/IR in F110W (top row). The 3-σ error ellipses on the precise position of the transient from new *HST*/WFC3 (solid) and Keck/NIRC2 (dashed) imaging are shown in white at the center of these panels. The nearest star-like object in the F814W image, labeled S1 in blue, is firmly outside the *HST* error ellipse. In the rightmost column, we show the *Spitzer*/IRAC archival [4.5] Super Mosaic (top), the most recent pre-explosion [4.5] image (center), and the subtraction of the two (bottom), clearly showing the variability of the coincident IR precursor source.

a Markov Chain Monte Carlo simulation to estimate the photometric uncertainties (Yao et al., in prep.). Measurements for a given filter taken the same night were then averaged.

Follow-up images in the g', r', i', and Y bands were obtained with the Sinistro cameras on the Las Cumbres Observatory (LCO; Brown et al. 2013) 1-m telescopes under the program NOAO2019A-011 (PI: N. Blagorodnova). The data were reduced at LCO using the Beautiful Algorithms to Normalize Zillions of Astronomical Images (BANZAI) pipeline (McCully et al. 2018). Photometry from the LCO $g'r'i'$-band images were computed with the image-subtraction pipeline described in Fremling et al. (2016), with template images from the Sloan Digital Sky Survey (SDSS; Ahn et al. 2014). The pipeline performs PSF-fitting photometry calibrated against several SDSS stars in the field. We performed aperture photometry on M51 OT2019-1 in the LCO Y-band, with the aperture radius set by the typical full width at half maximum (FWHM) of stars in the images, calibrated against several stars in the Pan-STARRS1 (PS1; Chambers et al. 2016) DR2 catalog (Flewelling et al. 2016).

Additional ground-based follow-up images were obtained in the optical and near-IR at several epochs using the Astrophysical Research Consortium Telescope Imaging Camera (ARCTIC; Huehnerhoff et al. 2016) and Near-Infrared Camera & Fabry-Perot Spectrometer (NICFPS; Vincent et al. 2003) on the Astrophysical Research Consortium (ARC) 3.5-m Telescope at Apache Point Observatory (APO), and the Wide Field Infrared Camera (WIRC; Wilson et al. 2003) on the 200-inch Hale Telescope (P200) at Palomar Observatory. Imaging of M51 at APO were obtained as part of a program to monitor 24 galaxies in the SPitzer Infrared Intensive Transients Survey (SPIRITS; PI M. Kasliwal; PIDs 10136, 11063, 13053). Optical $g'r'i'$ images were reduced in the standard fashion using bias, dark, and twilight flat-field frames. Our near-IR JHK_s imaging employed large dithers alternating between the target and a blank sky field approximately every minute to allow for accurate subtraction of the bright near-IR sky background, and individual frames were flat-fielded, background-subtracted, astrometrically aligned with a catalog of Two Micron All Sky Survey (2MASS; Skrutskie et al. 2006) sources, and stacked. We performed aperture photometry at the location of the transient, and used the $g'r'i'$ or JHK_s magnitudes of several isolated stars in SDSS or 2MASS to measure the photometric zero points in the optical and near-IR images, respectively.

Our photometry of M51 OT2019-1 is shown in Figure 2 on the AB magnitude system, corrected for Galactic extinction. Where appropriate we have converted $VRIJHK_s$ magnitudes on the Vega system to AB magnitudes using the conversions of Blanton & Roweis (2007).

We also obtained high-resolution, adaptive-optics J-band imaging of the transient on 2019 February 16.6, using the near-IR camera (NIRC2; PI K. Matthews) on the 10-m Keck II Telescope on Mauna Kea. Further high-resolution imaging was obtained on 2019 March 5.0 with the *Hubble Space Telescope* (*HST*) WFC3 camera in the F275W, F336W, and F814W filters as the first target in a test program proposing a new method of *HST* observing (PI A. Fruchter, PID SNAP-15675). This new method, called "Rolling Snapshots," allows fairly rapid response by updating a list of snapshot targets weekly; however, due to present limitations in the Astronomer's Proposal Tool (APT), the observing is done in a custom sub-array mode. Data were reduced using the standard pipelines at STScI, adding a charge-transfer-efficiency (CTE) correction (which was not done by the pipeline due to the use of the custom sub-array). CTE-corrected frames were then combined into image mosaics for each filter using AstroDrizzle within PyRAF to attempt to flag cosmic-ray hits. We performed PSF-fitting photometry for the transient using DOLPHOT (Dolphin 2000, 2016) and obtain 23.32 ± 0.17, 20.47 ± 0.03, and 15.754 ± 0.002 mag (Vega scale) for F275W, F336W, and F814W, respectively.

2.3. *Spectroscopic observations*

We obtained a sequence of optical spectra of M51 OT2019-1 using several instruments covering phases from $t = 4$ to 53 days. This includes four spectra with the Alhambra Faint Object Spectrograph and Camera (ALFOSC) on the 2.56-m Nordic Optical Telescope (NOT) at the Spanish Observatorio del Roque de los Muchachos on La Palma, including two low-resolution spectra with the 300 lines/mm grism (Gr4) and an epoch of intermediate-resolution spectra using two 600 lines/mm grisms (Gr7 & Gr8), three spectra with the Double Beam Spectrograph (DBSP; Oke & Gunn 1982) on P200, one spectrum with the Gemini Multi-Object Spectrograph (GMOS; Hook et al. 2004) on the Gemini North Telescope through our Target

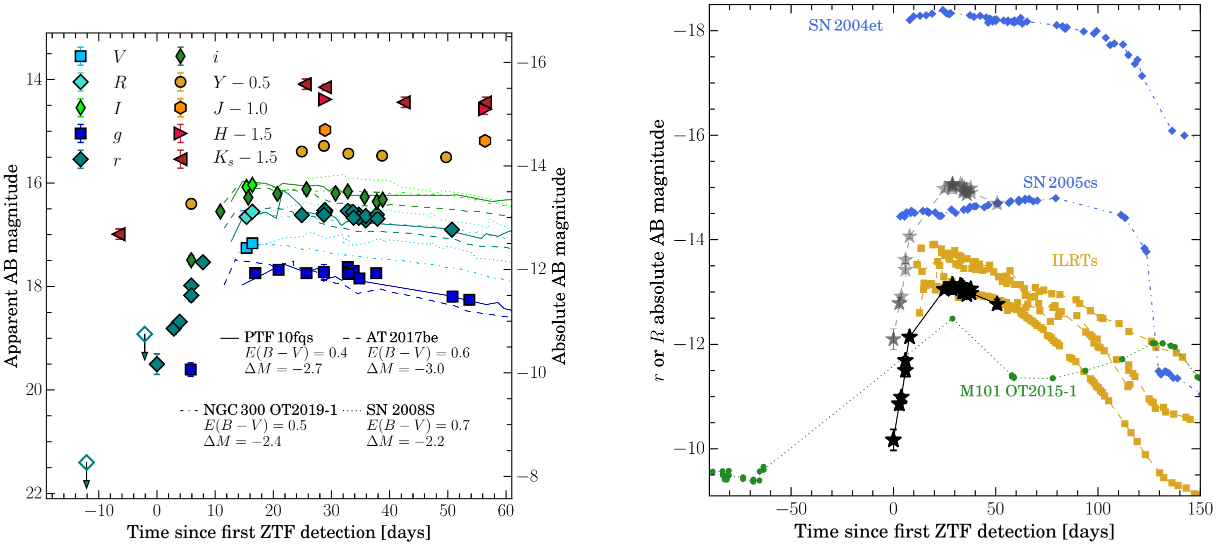

Figure 2. *Left:* Multi-band light curves of M51 OT2019-1 are shown as large filled symbols, and unfilled points with downward arrows represent upper limits from non-detections. Time on the x-axis is measured in days since the first detection by ZTF on 2019 January 22.6. We also show the VRI measurements reported by Pessev et al. (2019). Measurements have been corrected for Galactic extinction to M51 only, and $VRIJHK_s$ measurements have been converted from Johnson-Cousins/2MASS Vega magnitudes to AB magnitudes adopting Blanton & Roweis (2007) conversions. Absolute magnitudes at the assumed distance to M51 and assuming no host extinction are given on the y-axis to the right. For comparison, we show gri light curves of PTF10fqs (solid lines; Kasliwal et al. 2011), and the VRI light curves of SN 2008S (dotted lines; Botticella et al. 2009) and NGC300 OT2008-1 (dash-dotted lines, Humphreys et al. 2011). The comparison light curves have been corrected for Galactic extinction to their respective hosts from NED, then reddened to match the $g-r$ or $V-R$ colors of M51 OT2019-1 on the plateau and offset in absolute magnitude by the ΔM values indicated on the figure to match the vertical level of the M51 OT2019-1 light curves. *Right*: r-band light curves of M51 OT2019-1 are shown as the black stars, and corrected for our estimate of the total host/CSM extinction near peak with $E(B-V)=0.7$ mag as lighter gray stars. The r or R light curves of the comparison ILRTs are shown as yellow squares, also corrected with an estimate for the total extinction near peak as described in the text. We compare to the r or R-band light curves of other hydrogen-rich transients including the Type IIP SN 2004et (Maguire et al. 2010), low-luminosity Type IIP SN 2005cs (Pastorello et al. 2006), and the LRN M101 OT2015-1 (Blagorodnova et al. 2017).

of Opportunity program (PI: A. Miller; PID GN-2018B-Q-132), three spectra with the Spectral Energy Distribution Machine (SEDM; Blagorodnova et al. 2018) on the Palomar 60-in. Telescope (P60), and one spectrum with the Low Resolution Imaging Spectrometer (LRIS; Goodrich & Cohen 2003) on the Keck I Telescope. The spectra were reduced using standard techniques including wavelength calibration with arc-lamp spectra and flux calibration using spectrophotometric standard stars. In particular, we made use of a custom PyRAF-based reduction pipeline[2] (Bellm & Sesar 2016) for DBSP spectra, the IDL-based reduction and pipeline LPipe[3] (Perley 2019) for the LRIS spectrum, the fully automated Python-based reduction pipeline pysedm[4] (Rigault et al. 2019) for the SEDM spectra, and standard tasks in Gemini IRAF package[5] for the GMOS spectrum following procedures provided in the GMOS Data Reduction Cookbook[6].

---

[2] `https://github.com/ebellm/pyraf-dbsp`
[3] `http://www.astro.caltech.edu/~dperley/programs/lpipe.html`
[4] `https://github.com/MickaelRigault/pysedm`
[5] `http://www.gemini.edu/sciops/data-and-results/processing-software`
[6] `http://ast.noao.edu/sites/default/files/GMOS_Cookbook/`

We also obtained an epoch of near-IR spectroscopy of M51 OT2019-1 with the TripleSpec spectrograph (Herter et al. 2008) on P200. We obtained four exposures of the transient (300 s each) while nodding the transient along the slit between exposures to allow sky subtraction. The data were reduced with a modified version of the IDL-based data reduction package Spextool[7] (Cushing et al. 2004) for P200/TripleSpec. Corrections for the strong near-IR telluric absorption features and flux calibrations were performed with observations of the A0 V standard star HIP 61471, using the method developed by Vacca et al. (2003) implemented in the IDL tool xtellcor as part of Spextool.

A representative set of our spectral sequence is shown in Figure 3. All of our spectra will be made publicly available at the Weizmann Interactive Supernova Data Repository[8] (WISeREP; Yaron & Gal-Yam 2012).

3. ANALYSIS

3.1. *Archival imaging and progenitor constraints*

3.1.1. *Progenitor candidate identification*

We searched for the presence of a candidate progenitor star in archival imaging taken with *HST* and *Spitzer*/IRAC imaging. To determine the precise position of the transient in the archival *HST* imaging, we registered the NIRC2 *J*-band image of the transient with the 2015 ACS/WFC F814W image (PID: GO-13804, PI: K. McQuinn) and 2012 WFC3/IR F110W image (PID: 12490, PI: J. Koda). Using several stars and compact background galaxies in common between the new and archival frames, we achieved rms astrometric uncertainties on the position of the transient of 0.44 ACS pixels ($0''.022$) in the F814W image and 0.12 WFC3/IR pixels ($0''.015$) in the F110W image. We identified an apparent point source at the edge of our 3-σ error circle in the F814W image (object S1 in Figure 1), but the precision of our registration was insufficient to establish or rule out coincidence with the transient. We thus triggered the new *HST* observations with WFC3/UVIS, described above in Section 2.2, in order to obtain a more precise position.

We repeated the registrations as above, now using the new WFC3/UVIS F814W image and obtained improved rms astrometric uncertainties on the (x, y) position of the transient of $(0.13, 0.20)$ ACS pixels or $(0''.007, 0''.01)$ in the archival F814W image and 0.1 WFC3/IR pixels ($0''.01$) in the F110W image. We show the 3-σ error ellipses on the position of the transient in each of these images in Figure 1. We performed PSF-fitting photometry on the archival *HST* images used for registration using DOLPHOT. The nearest star detected in the 2015 F814W frame (object S1; $0''.06$ from the transient location) is firmly outside the 3-σ error ellipse. We note that there is an apparent source at the location of the transient in the archival F110W images, but it appears spatially extended and was not detected by DOLPHOT. Furthermore, the precise position of the transient is offset from the apparent centroid of this source. We thus find it is unlikely that the emission at the location is primarily due to the progenitor, and is more likely a blend of nearby, contaminating sources.

We then used DOLPHOT to obtain limits on the progenitor flux in the extensive archival coverage of the site with *HST*, including the images from 2005 with ACS/WFC in F435W, F555W, F814W, and F658N (PID: GO-10452; PI: S. Beckwith), 2012 with WFC3/UVIS in F689M and F673N (PID: GO-12762; PI: K. Kuntz), 2012 with WFC3/IR in F110W and F128N (PID: GO-12490; PI: J. Koda), 2014 with WFC3/UVIS in F275W and F336W (PID:GO-13340; PI: S. van Dyk), and 2015 with ACS/WFC in F606W and F814W (PID: GO-13804, PI: K. McQuinn). We adopt 5-σ limiting magnitudes based on the detection significance of the faintest sources from DOLPHOT within a 100-pixel radius of the transient position. Our full set limits

---

[7] `http://irtfweb.ifa.hawaii.edu/~cushing/spextool.html`
[8] `https://wiserep.weizmann.ac.il`

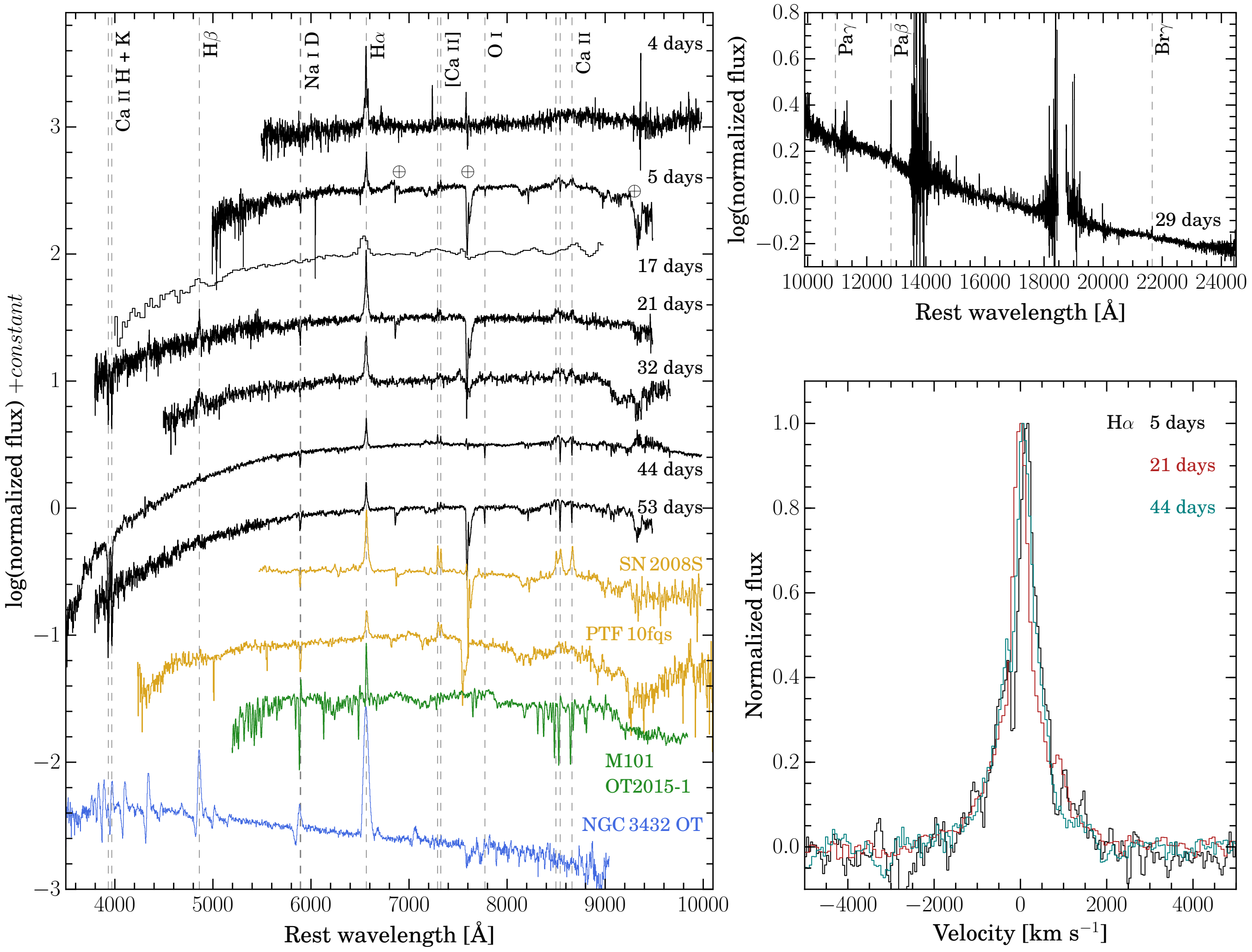

Figure 3. In the left panel, we show the optical spectral sequence of M51 OT2019-1 in black with the phase of each spectrum indicated along the right side of the panel. We show spectra of other ILRTs in yellow (SN 2008S from Botticella et al. 2009 and PTF 10fqs from Kasliwal et al. 2011), the M101 LRN (Blagorodnova et al. 2017) in green, and the 2008 LBV outburst in NGC 3432 (Pastorello et al. 2010) in blue for comparison. Each spectrum has been normalized to the continuum flux level around 7000 Å, and shifted vertically by an arbitrary constant for clarity. In the upper-right panel, we show the near-IR spectrum of M51 OT2019-1 from $t = 29$ days normalized to the continuum level around 16000 Å. We indicate the locations of several spectral features with gray, dashed vertical lines as labeled along the top of each panel. In the bottom right panel, we show the continuum-subtracted Hα velocity profiles for three representative epochs in the early evolution of the transient. The apparent absorption component in the $t = 5$ day spectrum is an artifact of the background subtraction.

on the progenitor from *HST* are shown in Figure 4, converted to band-luminosities (νL_ν) at the assumed distance to M51 and correcting for foreground Galactic extinction.

Utilizing the extensive archival coverage in the four imaging channels of the Infrared Array Camera (IRAC; Fazio et al. 2004) aboard *Spitzer* (Werner et al. 2004; Gehrz et al. 2007), we created deep stacks of all available images and registered them to the new *HST* imaging with an astrometric rms of $0.''4$. A source consistent with the position of M51 OT2019-1 ($0.''6$ away) is clearly detected in the [4.5] stack. We do not see a clear point source at the location in the other channel stacks. Based on aperture photometry the source has a [4.5] flux of 0.0177 ± 0.0048 mJy and 3-σ limiting fluxes of < 0.014, < 0.073, and < 0.31 mJy in [3.6], [5.8], and [8.0], respectively.

Using zero-magnitude fluxes (Vega system) given in the *Spitzer*/IRAC Handbook[9], we find this source to have $M_{[4.5]} = -12.2$ mag and $[3.6]-[4.5] > 0.74$ mag. If the [4.5] flux is indeed from the progenitor, the SED of M51 OT2019-1 may be similar to those of the self-obscured progenitors of SN 2008S and NGC 300 OT2008-1 (see Figure 4). The best-fit blackbody, incorporating the [4.5] detection and [3.6], [5.8], and [8.0] limits, has a temperature of $T \approx 510$ K and luminosity of $L \approx 6.3 \times 10^4\ L_\odot$. There is significant uncertainty in these parameters, however, and without constraints at longer wavelengths $> 10\ \mu$m, we are unable to rule out emission from cooler circumstellar dust that would indicate a more luminous (and hence more massive) progenitor.

3.1.2. *Pre-explosion variability*

We examined the considerable archival coverage of the location with *Spitzer*/IRAC at [3.6] and [4.5] for historical variability of the progenitor, including regular monitoring since 2014 as part of SPIRITS. The post-basic calibrated data (PBCD) level images were downloaded from the Spitzer Heritage Archive[10] and *Spitzer* Early Release Data Service[11] and processed through an automated image subtraction pipeline (for details see Kasliwal et al. 2017). For reference images, we used the available Super Mosaics[12] consisting of stacks of images obtained between 2004 May 18 and 2006 January 29.

Aperture photometry was performed at the location of M51 OT2019-1 in the difference images, and our resulting differential light curves are shown in Figure 5, converted to band-luminosities in νL_ν. During the years 2006–2008 ($\approx$ 3900–4400 days before discovery), our measurements are consistent with no change compared to the reference level within $|\Delta(\nu L_\nu)| \lesssim 10^4\ L_\odot$. In 2012 ($\approx$ 2400 days before discovery), we detect a significant, 4σ-level increase of $\Delta(\nu L_\nu) = (3.2 \pm 0.8) \times 10^4\ L_\odot$. Following this, in the time between 2014–2017 ($\approx$ 1600–500 days before discovery), we note a consistently elevated [4.5] flux at the location at $\Delta(\nu L_\nu) \approx 1.3 \times 10^4\ L_\odot$, although no individual epoch is detected at $> 3\sigma$ significance. In the final 2 epochs of *Spitzer* coverage, we detect a significant pre-explosion brightening starting sometime between $\approx$ 500 and 300 days before discovery, and rising to the level of $\Delta(\nu L_\nu) = (3.7 \pm 0.7) \times 10^4\ L_\odot$ at $t = -162.3$ days. At [3.6], the same trends in pre-explosion variability are evident, but at a lower level of significance.

We obtained constraints on pre-explosion optical variability at the location using the available coverage by the Palomar Transient Factory (Law et al. 2009; Rau et al. 2009) and its successor, the intermediate Palomar Transient Factory (i)PTF (Cao et al. 2016), and ZTF on P48. For (i)PTF g and Mould-R band data taken between 2009-2016 we utilized forced PSF-fitting photometry at the transient location on the reference-subtracted difference images (Masci et al. 2017). The same procedure as described in Section 2.2 was used to obtain photometry from ZTF difference images for the entire set of g and r-band coverage of the site in the Caltech and Partnership surveys since the start of full operations in March 2018. To obtain deeper limits, we stacked our measurements from (i)PTF and ZTF within 10-day windows, and show the resulting differential optical light curves along with the IR constraints in Figure 5. We see no evidence for significant optical variability at the location in any of the archival P48 coverage at the level of $|\Delta(\nu L\nu)| \lesssim 2 \times 10^4$ and $3 \times 10^4\ L_\odot$ in the R or r, and g-bands, respectively, including during the 2012 and 2017–2018 [4.5] brightening episodes.

---

[9] `https://irsa.ipac.caltech.edu/data/SPITZER/docs/irac/iracinstrumenthandbook/`

[10] `https://sha.ipac.caltech.edu/applications/Spitzer/SHA/`

[11] `http://ssc.spitzer.caltech.edu/warmmission/sus/mlist/archive/2015/msg007.txt`

[12] Super Mosaics are available as Spitzer Enhanced Imaging Products through the NASA/IPAC Infrared Science Archive: `https://irsa.ipac.caltech.edu/data/SPITZER/Enhanced/SEIP/overview.html`

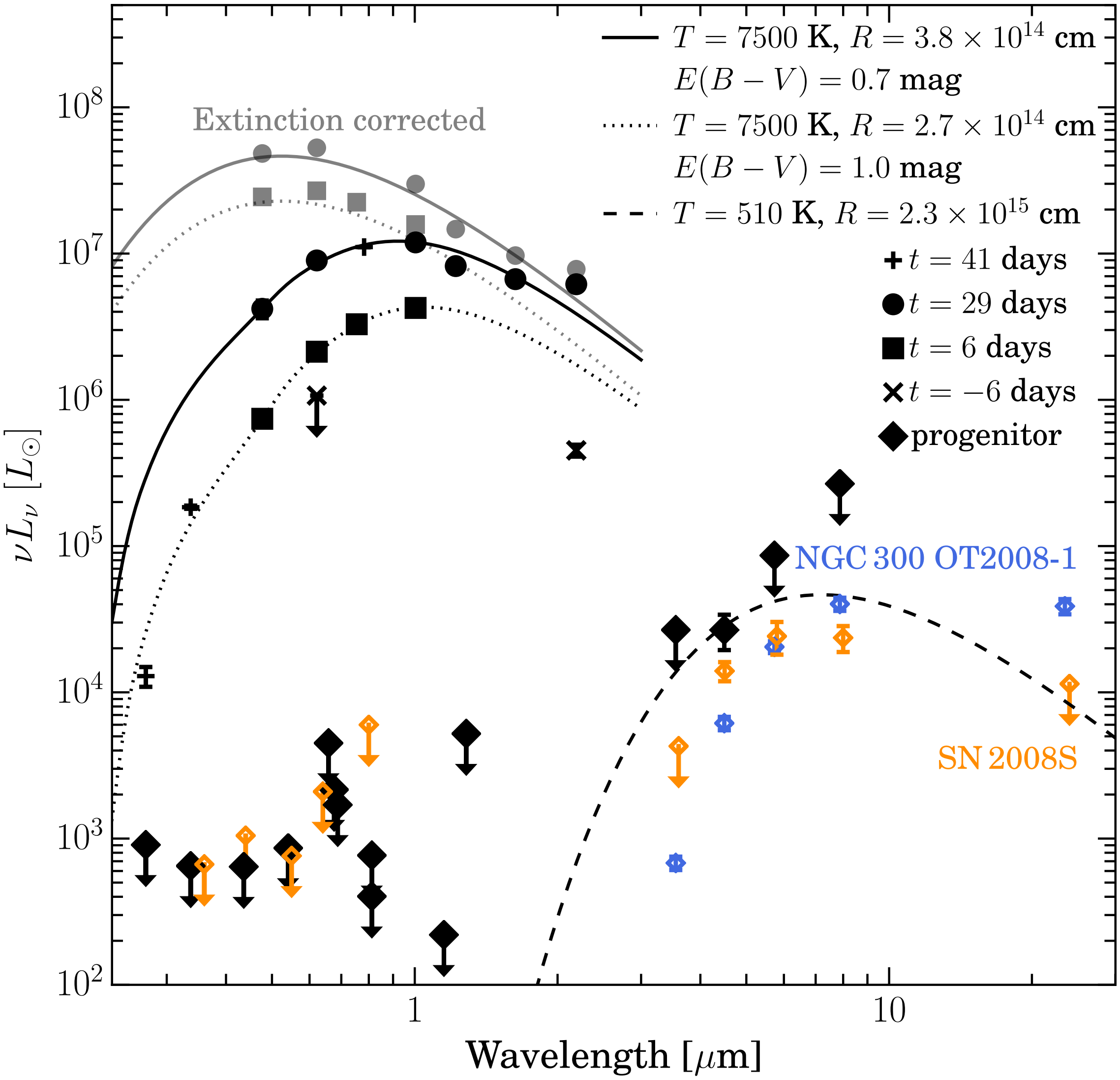

Figure 4. SEDs from photometry are shown in black for the M51 OT2019-1 progenitor (diamonds), and at multiple phases in the evolution of the transient ($t = -6$, 6, 29, and 41 days as "X"-symbols, squares, circles, and "+"-symbols, respectively). Upper limits from non-detections are indicated with downward arrows. Blackbody approximations to the data are shown for the progenitor (dashed curve), $t = 6$ day SED on the rise (dotted) and $t = 29$ day SED on the plateau with radii and temperatures given in the legend. For post-discovery SEDs of the transient, the curves shown have been reddened by the amount listed. The corresponding de-reddened data and blackbody curves are shown in gray. For comparison, the progenitor SED data are shown for NGC 300 OT2008-1 (open blue diamonds; Prieto 2008) and SN 2008S (open orange diamonds; Prieto et al. 2008).

3.2. *Photometric properties*

The multi-band optical and near-IR light curves of M51 OT2019-1 are shown in Figure 2. We observe a rise in the optical light curves over a time of ≈ 15 days after the first detection by ZTF, after which the source exhibits a relatively flat plateau in the g, r, i and Y band to at least $t = 40$ days. In the r band, the source is observed to peak at $M_r = -13.0$ (Galactic extinction correction only). The optical colors are remarkably red, with values on the rise of $g-r = 1.3 \pm 0.2$, $g-i = 1.9 \pm 0.2$, and $g-Y = 2.6 \pm 0.2$ mag at $t = 5.9$ days. On

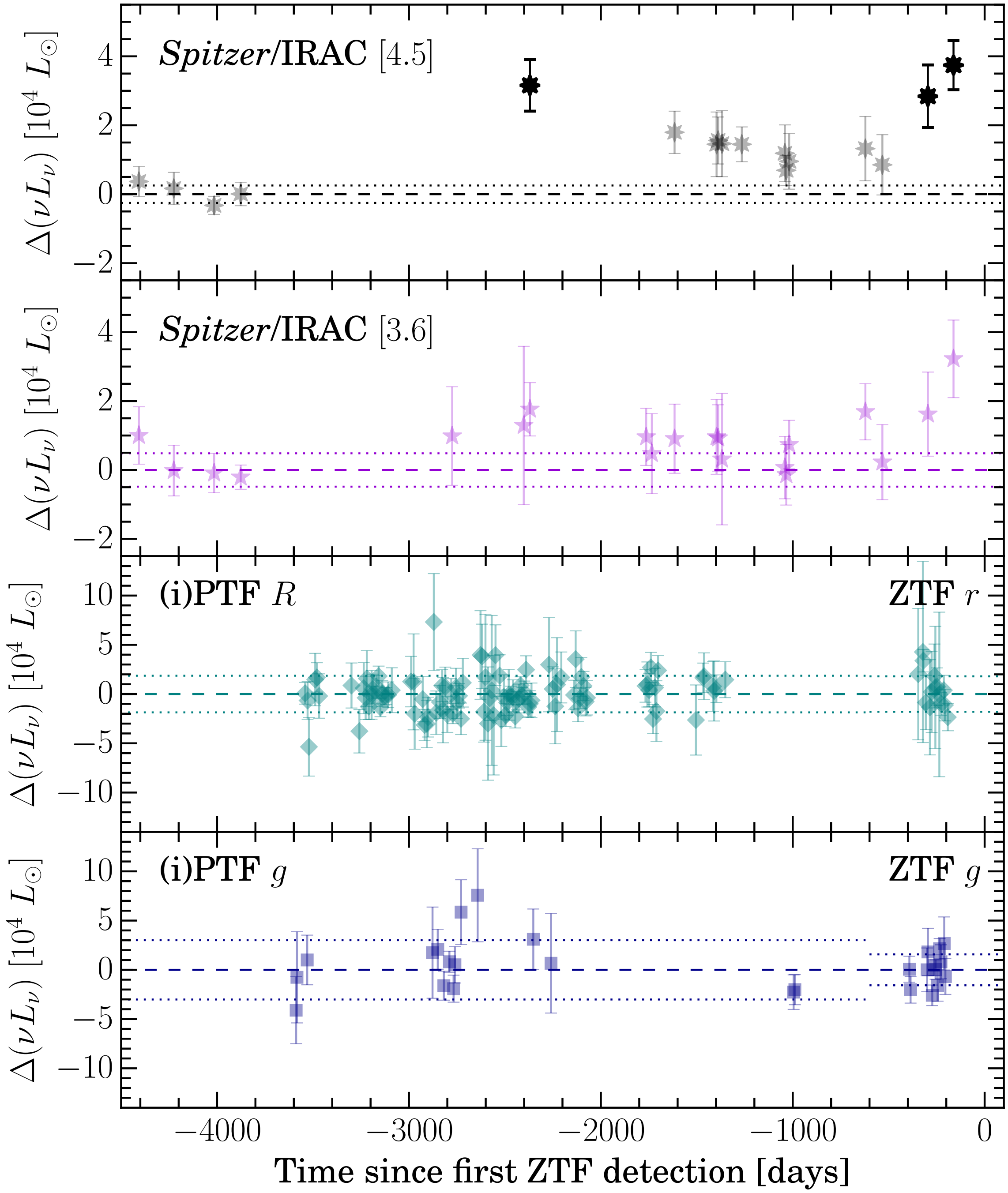

Figure 5. Constraints on pre-explosion variability based on image subtraction at the location of the transient in the IR with *Spitzer*/IRAC and optical with (i)PTF and ZTF. From top to bottom we show the differential light curves at the [4.5], [3.6], *R* or *r*, and *g* bands. Dashed lines indicate the zero-level, and dotted lines in each panel show the standard deviations of our measurement for the first four epochs of *Spitzer* imaging, and for the entire sets of (i)PTF and ZTF imaging. The darker, solid-black points in the [4.5] light curve highlight individual epochs where we detect variability of the progenitor at $> 3\sigma$ significance.

the plateau at $t = 25.9$ days, we observe bluer optical colors of $g-r = 0.97 \pm 0.05$, $g-i = 1.53 \pm 0.06$, and $g-Y = 1.8 \pm 0.1$ mag. In the near-IR, the source was detected 6.5 days before the earliest ZTF detection at $K_s = 18.2 \pm 0.3$, before rising to $K_s = 15.66 \pm 0.06$ at $t = 28.9$ days.

Given its red optical colors and location in a dark dust lane, it is likely that M51 OT2019-1 is subject to significant extinction. High amounts of optical extinction have also been inferred for similar transients of the ILRT class, but even among these, M51 OT2019-1 is exceptionally red. As shown in Figure 2, we estimate the excess reddening present in M51 OT2019-1 by comparing its optical light curves to those of the well studied ILRTs SN 2008S (Botticella et al. 2009), NGC 300 OT2008-1 (Humphreys et al. 2011), PTF 10fqs (Kasliwal et al. 2011), and AT 2017be (Cai et al. 2018). After correcting the light curves for Galactic extinction, we require *excess* reddening of $E(B-V) \approx 0.7$, 0.5, 0.4, and 0.6 mag for each of those objects, respectively, to match the optical colors of M51 OT2019-1 near peak on the plateau.

The total extinction to M51 OT2019-1 at a given phase is likely due to a combination of attenuation by foreground dust in the host interstellar medium (ISM) as well as internal extinction by dust in the circumstellar medium (CSM). For NGC 300 OT2008-1, Humphreys et al. (2011) estimated the total extinction near the peak of the transient as $E(B-V) \approx 0.4$ mag based on comparing its optical colors to those expected for a temperature $T \approx 7500$ K inferred from the presence of F-type absorption features in the spectrum. A similar argument was made by Smith et al. (2009) to estimate a total host/CSM extinction to SN 2008S of $E(B-V) = 0.28$ mag.

As described below in Section 3.3, we observe similar absorption features in the spectra of M51 OT2019-1 throughout its evolution, and thus infer a similar temperature for the continuum emission. Our analysis of the spectral energy distribution (SED) derived from photometry at several phases in the evolution of the transient is shown in Figure 4. We observed an early brightening at $t = -6$ days in the near-IR K_s-band to $\nu L_\nu \approx 4 \times 10^5\ L_\odot$ with a constraining r-band non-detection a few days later that suggests the explosion is heavily obscured at early times. At $t = 6$ days as the transient rises in the optical, comparing the SED to a reddened blackbody spectrum with $T = 7500$ K provides a good approximation to the data and suggests $E(B-V) = 1.0$ mag. Near the optical peak on the plateau at $t = 29$ days, the SED appears less reddened, and can be approximated by $T = 7500$ K with $E(B-V) = 0.7$ mag. While some amount of extinction can likely be attributed to foreground host extinction, the variable extinction estimate from evolution of the SED indicates a significant contribution from internal CSM dust. In particular, we suggest the color evolution of the SED from rise to peak may be attributed to the continued destruction of CSM dust as the explosion emerges from the dense obscuring wind of the progenitor.

The luminosity of the corresponding unreddened blackbody is $L = 8.3 \times 10^7\ L_\odot$, which we adopt as a crude estimate of the intrinsic bolometric luminosity of the explosion at peak. In comparison, the most luminous classical novae reached peak luminosities from ≈ 3–$8 \times 10^5\ L_\odot$ (Gallagher & Ney 1976; Gehrz et al. 2015), while typical CCSNe reach 5×10^8 to $\gtrsim 10^{10}\ L_\odot$ (e.g., Valenti et al. 2016). We note however, the reddened blackbody model significantly over-predicts the observed Y-band flux at this epoch. We also see evidence for an IR excess in the near-IR K_s-band measurement, suggesting emission from dust is an important component of the SED. Finally, in the SED at $t = 41$ days from our *HST* observations ("+"-symbols in Figure 4), the measurement in F814W lies near the expectation from the reddened blackbody approximation to the $t = 29$ day SED, consistent with the flat evolution of the i'-band light curves between these epochs; however, the F336W and F275W points are significantly below this expectation, suggesting that there may be additional suppression of the flux in the blue and UV (e.g., line blanketing) and/or that the assumed Fitzpatrick (1999) $R_V = 3.1$ extinction law for the diffuse Milky Way ISM may not applicable for heavy internal extinction by circumstellar dust, especially at bluer wavelengths. The addition of longer wavelength measurements and self-consistent modelling of the time evolution of the SED will be necessary to better constrain the intrinsic properties of the explosion and the surrounding CSM dust.

In the right panel of Figure 2, we compare the r-band light curve of M51 OT2019-1 to other hydrogen-rich transients. For the sample of ILRTs, we correct for an estimate of the total extinction based on the SED near peak as described above. Assuming $E(B-V) = 0.7$ mag for M51 OT2019-1, the peak absolute magnitude is $M_r \approx -15$. This is notably more luminous than the other proposed members of this class, which fall between $M_{r/R} \approx -13$ to -14, and is near the range more typical of Type II core-collapse SNe. In fact, with our assumed extinction, M51 OT2019-1 is even more luminous than some low-luminosity Type IIP SNe, e.g., SN 2005cs (Pastorello et al. 2006).

3.3. *Spectroscopic properties*

Our optical spectral sequence of M51 OT2019-1 from $t = 4$ to 53 days is shown in Figure 3. The spectra are characterized by a very red continuum, and display prominent Hα emission along with emission features of the Ca II IR triplet ($\lambda\lambda$ 8498, 8542, 8662) and [Ca II] ($\lambda\lambda$ 7291, 7324). We detect the Ca II H and K lines ($\lambda\lambda$ 3968, 3934), the Na I D doublet ($\lambda\lambda$ 5889, 5895), and a strong O I blend near 7773 Å in absorption. Superimposed on the broader emission features, we also detect a narrower absorption component for each of the lines of the Ca II triplet. In the near-IR spectrum at $t = 29$ days (upper-right panel of Figure 3), we see additional recombination lines of H in emission including Paβ and weaker Paγ.

These features indicate a wide range of densities in the gas producing the spectrum—reminiscent of a wind or ejected envelope with large inhomogeneities. The observed [Ca II] $\lambda\lambda$ 7291, 7324 lines have a critical density of $n_{cr} \sim 10^7$ cm^{-3} (Ferland & Persson 1989) and are strongly suppressed at higher densities. On the other hand, the O I λ7773 transition, a quintet frequently observed in transients, is normally populated by collisional transfer from the O I 3p ^{3}P level, which is itself strongly excited by a wavelength coincidence between the H I Ly-β and O I λ1026 transitions (Bowen 1947). The triplet-to-quintet collisional transfer is only effective at densities $n \gtrsim 10^{11}$ cm^{-3} (Williams 2012), thus demonstrating a wide range of densities in the gas ejected by the outburst.

The Hα velocity profiles (bottom-right panel of Figure 3) appear symmetric about their peaks, which are consistent with zero-velocity in the rest frame of M51. The profiles are characterized by a FWHM velocity of ≈ 400 km s^{-1} with broader electron-scattering wings extending to ≈ 2000 km s^{-1}. The $t = 5$ day GMOS spectrum shows an apparent absorption feature near ≈ -180 km s^{-1}, but we attribute this to a data reduction artifact from over-subtraction of unrelated, background Hα emission and difficultly in finding a suitably clean region for background subtraction along the slit. We do not see any evidence for significant evolution in the line profile shape or width for the duration of the observations presented here.

The observed absorption spectrum is reminiscent of an F-supergiant. This is expected for an eruption that produces an extended, optically-thick wind (Davidson 1987), and is seen in LBVs/S Doradus variables in their cool, outburst state at maximum (Humphreys & Davidson 1994), some SN impostors and LBV giant eruptions (e.g. Smith et al. 2011), and is very similar to that of NGC 300 OT2008-1 (Bond et al. 2009; Humphreys et al. 2011) and SN 2008S (Smith et al. 2009). This suggests a temperature of ≈ 7500 K. The red continuum is therefore suggestive of significant extinction, and we apply this temperature estimate to our SED analysis in Section 3.2 to obtain $E(B-V) = 0.7$ mag near the peak at $t = 29$ days. Overall, the spectral features described above are generally similar to some previously observed SN impostors and ILRTs.

4. DISCUSSION AND CONCLUSIONS

From our early observations of M51 OT2019-1 in the first ≈ 60 days of its evolution, we find that the transient is characterized by a ≈ 15 day rise in the optical to an observed plateau luminosity of $M_r = -13$ (Galactic extinction correction only). Its spectrum shows strong Hα emission with FWHM velocities of ≈ 400 km s^{-1}. These basic properties are similar to those of multiple classes of transients with luminosities intermediate between those of novae and supernovae, including ILRTs, LRNe, and giant eruptions of LBVs. The photometric evolution of M51 OT2019-1 has transitioned smoothly from the rise to a plateau lasting through at least $t \approx 50$ days, consistent with ILRTs and also similar to some SN impostors. It is more dissimilar to LRNe whose light curves are typically irregular and multi-peaked (Smith et al. 2016; Blagorodnova et al. 2017) and some other LBV eruptions that may how multiple outbursts or erratic variability (Pastorello et al. 2010; Smith et al. 2010). Our optical spectra show several additional features, including Ca II and [Ca II] in emission, F-type absorption features indicating the light is escaping an optically thick wind at ≈ 7500 K, and a red continuum indicative of significant extinction. These features are characteristic of ILRTs, but may also be seen in LRNe and giant LBV eruptions. For example, while some LBV eruptions show bluer continua and H lines with strong P Cygni profiles (e.g., NGC 3432 OT; Pastorello et al. 2010), others are indistinguishable from ILRTs (Smith et al. 2010, 2011; Rest et al. 2012; Prieto et al. 2014). We identify a likely progenitor star in archival *Spitzer* imaging with $M_{[4.5]} = -12.2$ mag and $[3.6]-[4.5] > 0.74$ mag, but there is no identifiable optical counterpart in archival *HST* imaging. This is reminiscent of properties of the obscured progenitors of SN 2008S and NGC 300 OT2008-1, and notably, stars with these IR properties are exceptionally rare (Thompson et al. 2009; Khan et al. 2010). We thus suggest M51 OT2019-1 is an ILRT. Without longer wavelength archival constraints, though, we cannot rule out that the progenitor of M51 OT2019-1 is more luminous and massive than the 9–15 $M_\odot$ stars inferred for the ILRT prototypes.

The nature of ILRTs, the mechanism behind their outbursts, and their relation to other impostors and LBV-related transients are debated. One proposed physical scenario involves a weak explosion, possibly the electron-capture-induced collapse of an extreme asymptotic-giant-branch star. In this scenario, an initial flash rapidly destroys the enshrouding circumstellar dust, which later reforms and re-obscures the optical transient (Thompson et al. 2009; Kochanek 2011; Szczygieł et al. 2012). Thanks to the early discovery of M51 2019OT-1, we find evidence for continued dust destruction during the rise of the transient as our estimate of the reddening evolves from $E(B-V) = 1.0$ to 0.7 mag between $t = 6$ and 29 days, posing a challenge to such interpretations for this event. Adopting $E(B-V) = 0.7$ mag at peak, the intrinsic luminosity is $M_r = -15$ mag, higher than previously observed ILRTs, though not unusual for some SN impostors (Smith et al. 2011). The observed variability of the likely progenitor may also hint at eruptive, self-obscuring episodes occurring in the years before the explosion. A full picture of the event awaits continued monitoring, including planned *Spitzer* observations, to characterize the full SED, dust properties, and energetics. Longer term, mid-IR spectroscopic observations with the *James Webb Space Telescope* will disentangle the chemistry, and late-time imaging after the explosion fades away will provide definitive evidence on whether the explosion was terminal.

This material is based upon work supported by the National Science Foundation Graduate Research Fellowship under Grant No. DGE-1144469. H.E.B. acknowledges support from program numbers GO-14258 and AR-15005, provided by NASA through grants from the Space Telescope Science Institute, which is operated by the Association of Universities for Research in Astronomy, Incorporated, under NASA contract NAS5-26555. This work is part of the research programme VENI, with project number 016.192.277, which is (partly) financed by the Netherlands Organisation for Scientific Research (NWO). A.G.-Y. is supported by the EU via ERC grant No. 725161, the ISF, the BSF Transformative program and by a Kimmel award. R.D.G. was supported by NASA and the United States Air Force. Based on observations obtained with the Samuel Oschin Telescope 48-inch and the 60-inch Telescope at the Palomar Observatory as part of the Zwicky Transient Facility project. ZTF is supported by the National Science Foundation under Grant No. AST-1440341 and a collaboration including Caltech, IPAC, the Weizmann Institute for Science, the Oskar Klein Center at Stockholm University, the University of Maryland, the University of Washington, Deutsches Elektronen-Synchrotron and Humboldt University, Los Alamos National Laboratories, the TANGO Consortium of Taiwan, the University of Wisconsin at Milwaukee, and Lawrence Berkeley National Laboratories. Operations are conducted by COO, IPAC, and UW. This work was supported by the GROWTH project funded by the National Science Foundation under Grant No 1545949. SED Machine is based upon work supported by the National Science Foundation under Grant No. 1106171. The work presented here is based on observations obtained with the Apache Point Observatory 3.5-meter telescope, which is owned and operated by the Astrophysical Research Consortium. We thank the Apache Point Observatory Observing Specialists for their assistance during the observations. The data presented here were obtained in part with ALFOSC, which is provided by the Instituto de Astrofisica de Andalucia (IAA) under a joint agreement with the University of Copenhagen and NOTSA. Based on observations obtained at the Gemini Observatory acquired through the Gemini Observatory Archive and processed using the Gemini IRAF package, which is operated by the Association of Universities for Research in Astronomy, Inc., under a cooperative agreement with the NSF on behalf of the Gemini partnership: the National Science Foundation (United States), National Research Council (Canada), CONICYT (Chile), Ministerio de Ciencia, Tecnología e Innovación Productiva (Argentina), Ministério da Ciência, Tecnologia e Inovação (Brazil), and Korea Astronomy and Space Science Institute (Republic of Korea). Some of the data presented herein were obtained at the W. M. Keck Observatory, which is operated as a scientific partnership among the California Institute of Technology, the University of California and the National Aeronautics and Space Administration. The Observatory was made possible by the generous financial support of the W. M. Keck Foundation. The authors wish to recognize and acknowledge the very significant cultural role and reverence that the summit of Maunakea has always had within the indigenous Hawaiian community. We are most fortunate to have the opportunity to conduct observations from this mountain. This work is based in part on observations made with the *Spitzer Space Telescope*, which is operated by the Jet Propulsion Laboratory, California Institute of Technology under a contract with NASA. Based on observations made with the NASA/ESA *Hubble Space Telescope*, obtained from the Data Archive at the Space Telescope Science Institute, which is operated by the Association of Universities for Research in Astronomy, Inc., under NASA contract NAS 5-26555. Some of these observations are associated with program #15675. This research has made use of the NASA/IPAC Extragalactic Database (NED), which is operated by the Jet Propulsion Laboratory, California Institute of Technology, under contract with the National Aeronautics and Space Administration.

Facilities: PO:1.2m (ZTF), PO:1.5m (SEDM), Hale (DBSP, WIRC, TripleSpec), NOT (ALFOSC), Gemini:Gillett (GMOS), Keck:I (LRIS), Keck:II (NIRC2), ARC (NICFPS, ARCTIC), Spitzer (IRAC), HST (ACS, WFC3).

Software: AstroDrizzle (Hack et al. 2012, `http://drizzlepac.stsci.edu`), DOLPHOT (Dolphin 2000, 2016), IRAF (Tody 1986, 1993), Gemini IRAF package (`http://www.gemini.edu/sciops/data-and-results/processing-software`), PyRAF (`http://www.stsci.edu/institute/software_hardware/pyraf`), pyraf-dbsp (Bellm & Sesar 2016, `https://github.`

com/ebellm/pyraf-dbsp), LPipe (Perley 2019, http://www.astro.caltech.edu/~dperley/programs/lpipe.html).

REFERENCES

Adams, S. M., Kochanek, C. S., Prieto, J. L., et al. 2016, MNRAS, 460, 1645

Ahn, C. P., Alexandroff, R., Allende Prieto, C., et al. 2014, ApJS, 211, 17

Bellm, E. C., & Sesar, B. 2016, pyraf-dbsp: Reduction pipeline for the Palomar Double Beam Spectrograph, Astrophysics Source Code Library, ascl:1602.002

Bellm, E. C., Kulkarni, S. R., Graham, M. J., et al. 2019, PASP, 131, 018002

Berger, E., Soderberg, A. M., Chevalier, R. A., et al. 2009, ApJ, 699, 1850

Blagorodnova, N., Kotak, R., Polshaw, J., et al. 2017, ApJ, 834, 107

Blagorodnova, N., Neill, J. D., Walters, R., et al. 2018, PASP, 130, 035003

Blanton, M. R., & Roweis, S. 2007, AJ, 133, 734

Bond, H. E. 2011, ApJ, 737, 17

Bond, H. E., Bedin, L. R., Bonanos, A. Z., et al. 2009, ApJL, 695, L154

Bond, H. E., & Siegel, M. H. 2006, AJ, 131, 984

Bond, H. E., Henden, A., Levay, Z. G., et al. 2003, Nature, 422, 405

Botticella, M. T., Pastorello, A., Smartt, S. J., et al. 2009, MNRAS, 398, 1041

Bowen, I. S. 1947, PASP, 59, 196

Brown, T. M., Baliber, N., Bianco, F. B., et al. 2013, PASP, 125, 1031

Burke, J., Howell, D. A., Arcavi, I., et al. 2019, Transient Name Server Classification Report, 328

Cai, Y.-Z., Pastorello, A., Fraser, M., et al. 2018, MNRAS, 480, 3424

Cao, Y., Nugent, P. E., & Kasliwal, M. M. 2016, PASP, 128, 114502

Chambers, K. C., Magnier, E. A., Metcalfe, N., et al. 2016, arXiv e-prints, arXiv:1612.05560 [astro-ph.IM]

Cushing, M. C., Vacca, W. D., & Rayner, J. T. 2004, PASP, 116, 362

Davidson, K. 1987, ApJ, 317, 760

De, K., Tartaglia, L., Andreoni, I., et al. 2019, The Astronomer's Telegram, 12433

Dolphin, A. 2016, DOLPHOT: Stellar photometry, Astrophysics Source Code Library, ascl:1608.013

Dolphin, A. E. 2000, PASP, 112, 1383

Fazio, G. G., Hora, J. L., Allen, L. E., et al. 2004, ApJS, 154, 10

Ferland, G. J., & Persson, S. E. 1989, ApJ, 347, 656

Fitzpatrick, E. L. 1999, PASP, 111, 63

Flewelling, H. A., Magnier, E. A., Chambers, K. C., et al. 2016, arXiv e-prints, arXiv:1612.05243 [astro-ph.IM]

Fremling, C., Sollerman, J., Taddia, F., et al. 2016, ArXiv e-prints, arXiv:1606.03074 [astro-ph.HE]

Gallagher, J. S., & Ney, E. P. 1976, ApJL, 204, L35

Gehrz, R. D., Roellig, T. L., Werner, M. W., et al. 2007, Review of Scientific Instruments, 78, 011302

Gehrz, R. D., Evans, A., Helton, L. A., et al. 2015, ApJ, 812, 132

Goodrich, R., & Cohen, M. 2003, in Proc. SPIE, Vol. 4843, Polarimetry in Astronomy, ed. S. Fineschi, 146

Graham, M. J., Kulkarni, S. R., Bellm, E. C., et al. 2019, arXiv e-prints, arXiv:1902.01945 [astro-ph.IM]

Hack, W. J., Dencheva, N., Fruchter, A. S., et al. 2012, in American Astronomical Society Meeting Abstracts, Vol. 220, American Astronomical Society Meeting Abstracts #220, 135.15

Herter, T. L., Henderson, C. P., Wilson, J. C., et al. 2008, in Proc. SPIE, Vol. 7014, Ground-based and Airborne Instrumentation for Astronomy II, 70140X

Hook, I. M., Jørgensen, I., Allington-Smith, J. R., et al. 2004, PASP, 116, 425

Huehnerhoff, J., Ketzeback, W., Bradley, A., et al. 2016, in Proc. SPIE, Vol. 9908, Ground-based and Airborne Instrumentation for Astronomy VI, 99085H

Humphreys, R. M., Bond, H. E., Bedin, L. R., et al. 2011, ApJ, 743, 118

Humphreys, R. M., & Davidson, K. 1994, PASP, 106, 1025

Humphreys, R. M., Davidson, K., & Smith, N. 1999, PASP, 111, 1124

Kasliwal, M. M., Kulkarni, S. R., Arcavi, I., et al. 2011, ApJ, 730, 134

Kasliwal, M. M., Bally, J., Masci, F., et al. 2017, ApJ, 839, 88

Kasliwal, M. M., Cannella, C., Bagdasaryan, A., et al. 2019, PASP, 131, 038003

Khan, R., Stanek, K. Z., Prieto, J. L., et al. 2010, ApJ, 715, 1094

Kochanek, C. S. 2011, ApJ, 741, 37

Kulkarni, S. R., Ofek, E. O., Rau, A., et al. 2007, Nature, 447, 458

Law, N. M., Kulkarni, S. R., Dekany, R. G., et al. 2009, PASP, 121, 1395

Maguire, K., Di Carlo, E., Smartt, S. J., et al. 2010, MNRAS, 404, 981

Mahabal, A., Rebbapragada, U., Walters, R., et al. 2019, PASP, 131, 038002

Masci, F. J., Laher, R. R., Rebbapragada, U. D., et al. 2017, PASP, 129, 014002

Masci, F. J., Laher, R. R., Rusholme, B., et al. 2019, PASP, 131, 018003

McCully, C., Volgenau, N. H., Harbeck, D.-R., et al. 2018, in Society of Photo-Optical Instrumentation Engineers (SPIE) Conference Series, Vol. 10707, Software and Cyberinfrastructure for Astronomy V, 107070K

McQuinn, K. B. W., Skillman, E. D., Dolphin, A. E., Berg, D., & Kennicutt, R. 2016, ApJ, 826, 21

—. 2017, AJ, 154, 51

Modjaz, M., Kirshner, R., Challis, P., & Hutchins, R. 2005, IAUC, 8555

Nordin, J., Brinnel, V., Giomi, M., et al. 2019a, Transient Name Server Discovery Report, 141

Nordin, J., Brinnel, V., van Santen, J., et al. 2019b, arXiv e-prints, arXiv:1904.05922 [astro-ph.IM]

Oke, J. B., & Gunn, J. E. 1982, PASP, 94, 586

Pastorello, A., Sauer, D., Taubenberger, S., et al. 2006, MNRAS, 370, 1752

Pastorello, A., Botticella, M. T., Trundle, C., et al. 2010, MNRAS, 408, 181

Patterson, M. T., Bellm, E. C., Rusholme, B., et al. 2019, PASP, 131, 018001

Perley, D. A. 2019, arXiv e-prints, arXiv:1903.07629 [astro-ph.IM]

Pessev, P., Jones, D., Pejcha, O., et al. 2019, The Astronomer's Telegram, 12506

Prieto, J. L. 2008, The Astronomer's Telegram, 1550

Prieto, J. L., Kistler, M. D., Thompson, T. A., et al. 2008, ApJL, 681, L9

Prieto, J. L., Rest, A., Bianco, F. B., et al. 2014, ApJL, 787, L8

Rau, A., Kulkarni, S. R., Law, N. M., et al. 2009, PASP, 121, 1334

Rest, A., Prieto, J. L., Walborn, N. R., et al. 2012, Nature, 482, 375

Rich, R. M., Mould, J., Picard, A., Frogel, J. A., & Davies, R. 1989, ApJL, 341, L51

Rigault, M., Neill, J. D., Blagorodnova, N., et al. 2019, arXiv e-prints, arXiv:1902.08526 [astro-ph.IM]

Rizzi, L., Tully, R. B., Makarov, D., et al. 2007, ApJ, 661, 815

Schlafly, E. F., & Finkbeiner, D. P. 2011, ApJ, 737, 103

Schlegel, D. J., Finkbeiner, D. P., & Davis, M. 1998, ApJ, 500, 525

Schmidt, B., Kirshner, R., Peters, J., & Bernstein, G. 1994, IAUC, 5962

Silverman, J. M., Filippenko, A. V., & Cenko, S. B. 2011, The Astronomer's Telegram, 3398

Skrutskie, M. F., Cutri, R. M., Stiening, R., et al. 2006, AJ, 131, 1163

Smith, N. 2014, ARA&A, 52, 487

Smith, N., Li, W., Silverman, J. M., Ganeshalingam, M., & Filippenko, A. V. 2011, MNRAS, 415, 773

Smith, N., & Owocki, S. P. 2006, ApJL, 645, L45

Smith, N., Ganeshalingam, M., Chornock, R., et al. 2009, ApJL, 697, L49

Smith, N., Miller, A., Li, W., et al. 2010, AJ, 139, 1451

Smith, N., Andrews, J. E., Van Dyk, S. D., et al. 2016, MNRAS, 458, 950

Sparks, W. B., Bond, H. E., Cracraft, M., et al. 2008, AJ, 135, 605

Szczygieł, D. M., Prieto, J. L., Kochanek, C. S., et al. 2012, ApJ, 750, 77

Tachibana, Y., & Miller, A. A. 2018, PASP, 130, 128001

Thompson, T. A., Prieto, J. L., Stanek, K. Z., et al. 2009, ApJ, 705, 1364

Tody, D. 1986, in Proc. SPIE, Vol. 627, Instrumentation in astronomy VI, ed. D. L. Crawford, 733

Tody, D. 1993, in Astronomical Society of the Pacific Conference Series, Vol. 52, Astronomical Data Analysis Software and Systems II, ed. R. J. Hanisch, R. J. V. Brissenden, & J. Barnes, 173

Tonry, J. L., Denneau, L., Heinze, A. N., et al. 2018, PASP, 130, 064505

Tylenda, R., Hajduk, M., Kamiński, T., et al. 2011, A&A, 528, A114

Vacca, W. D., Cushing, M. C., & Rayner, J. T. 2003, PASP, 115, 389

Valenti, S., Howell, D. A., Stritzinger, M. D., et al. 2016, MNRAS, 459, 3939

Van Dyk, S. D., Peng, C. Y., King, J. Y., et al. 2000, PASP, 112, 1532

Vincent, M. B., Morse, J. A., Beland, S., et al. 2003, in Proc. SPIE, Vol. 4841, Instrument Design and Performance for Optical/Infrared Ground-based Telescopes, ed. M. Iye & A. F. M. Moorwood, 367

Werner, M. W., Roellig, T. L., Low, F. J., et al. 2004, ApJS, 154, 1

Williams, R. 2012, AJ, 144, 98

Wilson, J. C., Eikenberry, S. S., Henderson, C. P., et al. 2003, in Proc. SPIE, Vol. 4841, Instrument Design and Performance for Optical/Infrared Ground-based Telescopes, ed. M. Iye & A. F. M. Moorwood, 451

Yaron, O., & Gal-Yam, A. 2012, PASP, 124, 668